Appl. Phys. A 83, 341–346 (2006)
DOI: 10.1007/s00339-006-3502-7

Applied Physics A
Materials Science & Processing

B.R. TULL[1,✉]
J.E. CAREY[1]
M.A. SHEEHY[2]
C. FRIEND[1,2]
E. MAZUR[1]

Formation of silicon nanoparticles and web-like aggregates by femtosecond laser ablation in a background gas

[1] Division of Engineering and Applied Sciences, Harvard University, 9 Oxford Street, Cambridge, Massachusetts 02138, USA
[2] Department of Chemistry and Chemical Biology, Harvard University, 12 Oxford Street, Mb22, Cambridge, Massachusetts 02138, USA

Received: 31 August 2005/Accepted: 9 January 2006
Published online: 1 March 2006 •

ABSTRACT We show that the mechanism of nanoparticle formation during femtosecond laser ablation of silicon is affected by the presence of a background gas. Femtosecond laser ablation of silicon in a H_2 or H_2S background gas yields a mixture of crystalline and amorphous nanoparticles. The crystalline nanoparticles form via a thermal mechanism of nucleation and growth. The amorphous material has smaller features and forms at a higher cooling rate than the crystalline nanoparticles. The background gas also results in the suspension of plume material in the gas for extended periods, resulting in the formation (on a thin film carbon substrate) of unusual aggregated structures including nanoscale webs that span tears in the film. The presence of a background gas provides additional control of the structure and composition of the nanoparticles during short pulse laser ablation.

PACS 81.16.-c

1 Introduction

Femtosecond laser ablation is the explosive removal of material excited to extreme temperatures and pressures through absorption of a high-intensity laser pulse of subpicosecond duration. The femtosecond laser ablation of metals and semiconductors in a vacuum environment has been investigated extensively [1–6]. Recent research has focused on the formation mechanism of silicon nanoparticles created by the irradiation of silicon in vacuum with 800-nm, laser pulses of 80- to 200-fs duration [3–6]. Hydrodynamic models suggest that the nanoparticles form via mechanical fragmentation of a highly pressurized fluid undergoing rapid quenching during expansion in the vacuum [3]. Experimental studies of the evolution of the ablated silicon support this theoretical prediction and show that the ablated material is composed almost entirely of ejected liquid silicon with very little vapor [4, 6]. In addition, it was found that the nanoparticles form within 50 ps by a non-equilibrium, non-thermal phase transformation rather than by a thermal nucleation and growth process [6].

In this paper we present work on the irradiation of silicon with 800-nm, 100-fs laser pulses in a background gas of hydrogen (H_2) or hydrogen sulfide (H_2S). Our results indicate that the presence of the background gas during irradiation fundamentally changes the mechanism for nanoparticle formation. We observe two phases in the collected plume material: spherical particles of crystalline silicon ranging in diameter from 5 to 300 nm and a highly porous network of amorphous silicon with feature sizes ranging from 1 to 10 nm. We find that the crystalline nanoparticles form by thermal nucleation and growth; the amorphous phase forms from small droplets of liquid that are subjected to a high cooling rate. The size distribution of the crystalline nanoparticles is log-normal – that is, the logarithm of the particle diameter has a Gaussian distribution – suggesting that the ejected material initially contains a vapor component instead of consisting of just liquid droplets as observed in vacuum [6]. The presence of the background gas also gives rise to the formation of unusual webs of nanoparticles on the collection substrate. Our results indicate that the background gas affords additional control of the structure and composition of the nanoparticles.

2 Methods

The ablation plume was generated by irradiating a Si(111) wafer (n-type, $\varrho = 8$–$12\ \Omega\,\mathrm{m}$) with a 1-kHz train of 100-fs, 800-nm laser pulses produced by a regeneratively amplified Ti:sapphire laser. The silicon wafer was placed in a stainless steel vacuum chamber, evacuated to about 6.7 Pa and then filled with either H_2 or H_2S to various pressures. The laser pulses were focused onto the silicon to a diameter of 150 μm yielding a peak fluence of $10\ \mathrm{kJ/m^2}$ and a peak intensity of about $10^{17}\ \mathrm{W/m^2}$. The plume material was collected over the course of 1 h as the silicon wafer was translated at a speed of 250 μm/s to prevent degradation of the target. This translation speed resulted in an average of 600 pulses delivered to each spot on the surface.

✉ Fax: +1-617-496-4654, E-mail: tull@fas.harvard.edu

We used transmission electron microscope specimen grids (3-mm-diameter, 200-mesh copper grids, coated on one side with a 20-nm-thick film of amorphous carbon) to collect material in the plume. The plane of the grids was perpendicular to the silicon surface and they were suspended above and in front of the silicon target with 18 gauge copper wire and carbon tape. The grids were positioned 10 mm from the target with the carbon-coated side facing down.

3 Results

We irradiated single crystal silicon wafers with a 1-kHz train of 800-nm, 100-fs laser pulses focused to a fluence of $10\,kJ/m^2$ in a chamber filled with H_2, or H_2S at a pressure of 67 kPa. We visually observed the ablation plume and collected the ejected material on transmission electron microscope (TEM) specimen grids positioned 10 mm from the target. The size, structure, and composition of the collected nanoparticles were determined using bright and dark field imaging, selected area diffraction, and energy dispersive spectroscopy in a transmission electron microscope.

The background gas influences the shape and trajectory of the ablation plume. At a 1-kHz pulse rate, the ablation plume appears as a constant stream of ejected material in the shape of a cone, which expands from the 150-μm-diameter laser-irradiated spot to millimeter dimensions making it readily visible to the eye. In contrast to vacuum, where the ejected material retains most of its initial kinetic energy until it impacts a surface, the background gas reduces the kinetic energy of the ejected material to zero. The material then remains suspended in the background gas for the duration of the experiment and travels around the chamber by convection. When H_2S is used as the background gas, the ablation plume is a narrow cone that initially travels perpendicular to the silicon surface and then curves upward until it comes to a stop and begins to fall back down. When H_2 is the background gas, the ablation plume is a wider cone that remains perpendicular to the silicon surface until it eventually slows to a stop and then travels around the chamber by convection.

Although the trajectory of the ablation plume is different for irradiation in both H_2S and H_2, the size and the structure of the collected material is the same. The TEM bright field image in Fig. 1a shows that the collected material is composed of an extremely fine network of aggregated material. The network consists of clusters of spherical particles, ranging in diameter from 5 to 300 nm, dispersed in a highly porous material with feature sizes ranging from 1 to 10 nm(Fig. 1b). In Fig. 1b, the spherical particles vary in brightness from light gray to deep black. In bright field imaging, a low brightness indicates that the material is highly diffracting [7]. When imaging the spherical particles, they alternate between gray and black on the time scale of seconds. This observation supports the hypothesis that the particles are single crystals; the alternating brightness is caused by the particles tilting in and out of the diffraction condition when they collect charge in the electron microscope. In comparison, the brightness of the highly porous material does not vary with time and appears between light gray and dark gray depending on the thickness of accumulated material.

Figure 2a shows a TEM bright field image showing the spherical particles on the left and the highly porous material on the right. Figure 2b and c show electron diffraction patterns obtained using the selected area diffraction apertures indicated by the corresponding circles in Fig. 2a. The diffraction pattern in Fig. 2b is characteristic of a polycrystalline material and the relative diameters of the rings confirm that the crystal structure of the spherical particles is diamond cubic. By positioning the selected area diffraction aperture over an individual particle, we verified that each

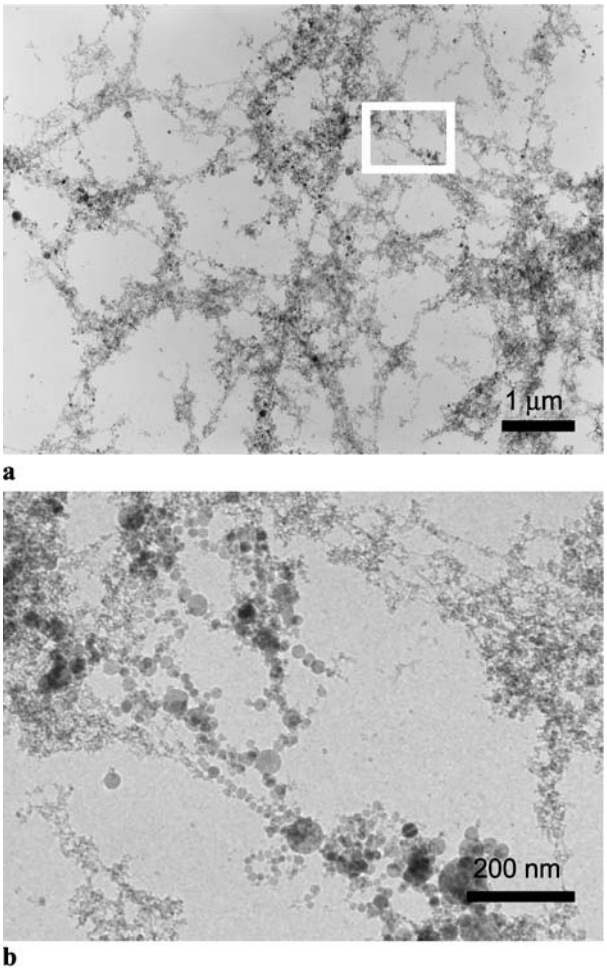

FIGURE 1 (**a**) Low magnification TEM bright field image showing particles formed in the ablation plume of silicon irradiated with trains of femtosecond laser pulses in H_2 at 67 kPa. (**b**) Higher magnification of the highlighted area in (**a**) reveals a network composed of spherical particles and porous material

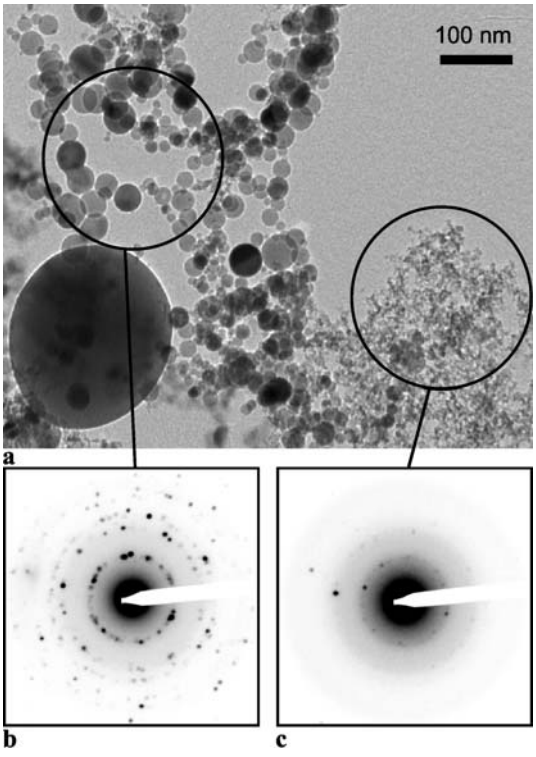

FIGURE 2 (**a**) TEM bright field image of particles generated in the ablation plume of silicon irradiated in H_2 at 67 kPa. Selected area diffraction reveals that (**b**) the spherical particles are crystalline and (**c**) the porous material is amorphous

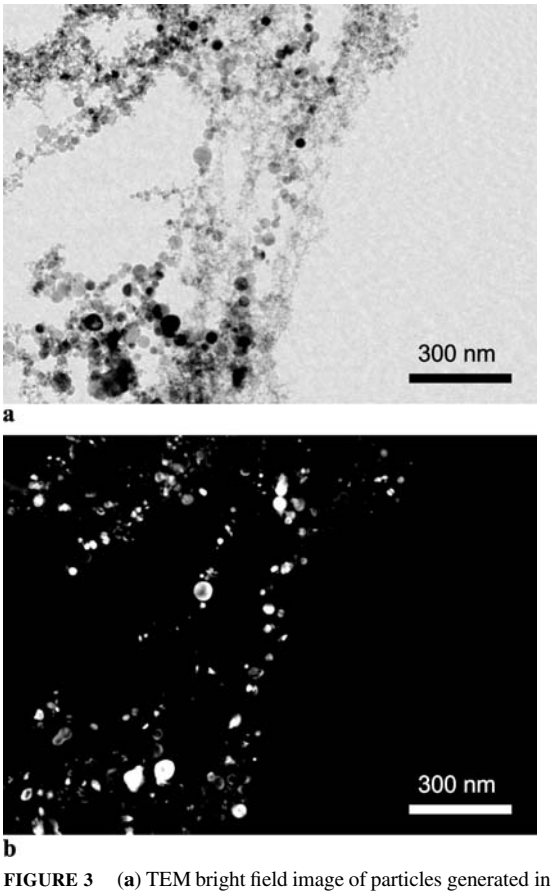

FIGURE 3 (**a**) TEM bright field image of particles generated in the ablation plume of silicon irradiated in H_2 at 67 kPa. (**b**) Compilation of eight dark field images acquired with the TEM C2 aperture positioned at eight different locations along the (111) diffraction ring. The bright areas indicate the locations of crystalline material

particle is actually a single crystal and that the diffraction pattern in Fig. 2b is the result of an ensemble of single crystal particles each at a different orientation. In contrast, Fig. 2c shows a diffraction pattern nearly absent of diffraction peaks, indicating an amorphous structure. The presence of a few diffraction peaks is due to crystalline particles mixed in with the amorphous material. Closer inspection of the image in Fig. 2a confirms the presence of a few crystalline particles in the amorphous material.

The bright and dark field TEM images in Fig. 3 confirm that the highly porous material is amorphous. Figure 3a shows a bright field image showing a mixture of spherical particles and highly porous material. Figure 3b is formed by a compilation of eight dark field images acquired with the TEM C2 aperture positioned at different locations around the first ring of the diffraction pattern in Fig. 2b. The first diffraction ring is populated by crystalline reflections from (111)-type planes. In each of the eight images, different spherical particles appear bright depending on whether their crystalline orientation produces a (111)-type reflection (e.g. each of the twelve [011] and twenty four [112] orientations in a diamond cubic crystal produces a (111)-type reflection). Crystalline particles that do not appear bright in Fig. 3b are likely oriented along a direction that does not produce a (111) reflection at any of eight locations. In contrast, the highly porous material is a uniform dark gray in all eight images, confirming that it is amorphous. If the highly porous material were crystalline, it would be unlikely that no part of that material produces a (111) reflection in any of the eight orientations.

The dark field images used to form Fig. 3b were compiled in the following manner. In seven of the eight images, the lower fourth of the brightness scale was subtracted. This removed the dark gray amorphous material from each image and left the bright crystalline particles behind. These images were then summed together and then added to the eighth image (which was unaltered) to produce Fig. 3b. By performing the sum in this manner, the relative brightness between the spherical particles and the amorphous phase in Fig. 3b is repre-

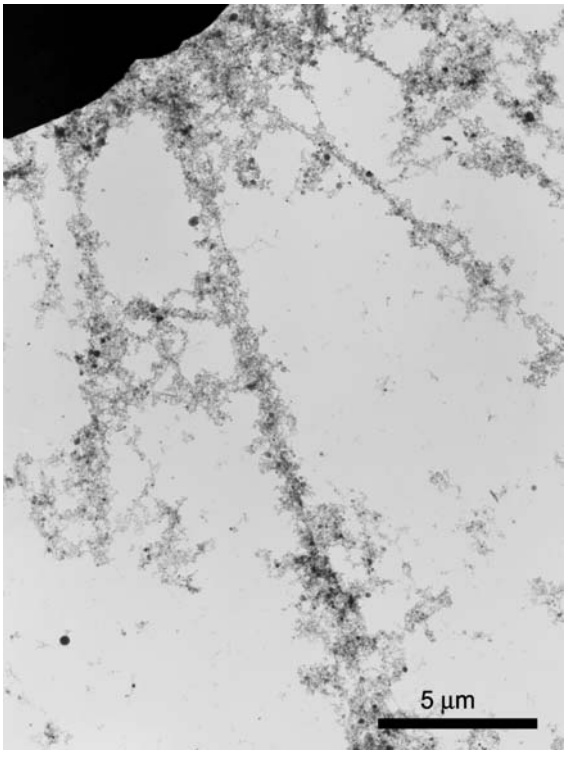

FIGURE 4 TEM bright field image showing how particles aggregate in straight lines measuring over 30 μm in length

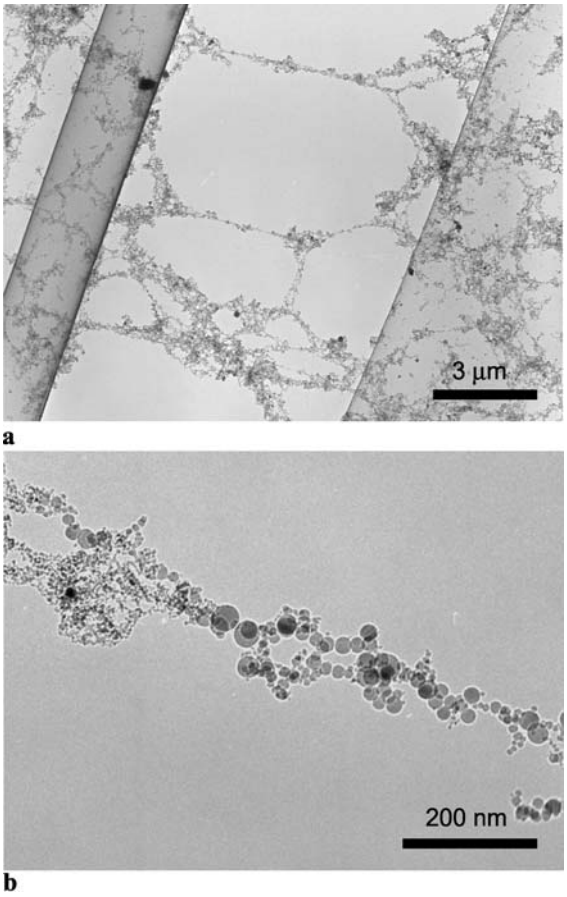

FIGURE 5 (**a**) Low magnification TEM bright field image showing particles forming nanoscale webs that span 10-μm-wide gaps in the collection substrate. (**b**) Higher magnification TEM bright field image showing that the bridges are composed of both crystalline and amorphous particles

sentative of each of the eight dark field images.

Using energy dispersive spectroscopy we find that the main component of both the crystalline particles and the amorphous material is silicon. Trace amounts of oxygen, carbon, and sulfur are detected in the amorphous material, and to a lesser extent in the crystalline particles. Sulfur is only detected when H_2S is used as the background gas. The presence of oxygen and carbon can be attributed to oxidation and contamination during transportation of the TEM specimen grids from the vacuum chamber to the TEM.

Figures 4 and 5 show aggregated material on copper TEM specimen grids coated with a smooth continuous carbon film. Figure 4 shows several strands of particles over 30 μm in length. The strands also span 10-μm-wide rips in the continuous carbon film like the strands of a web (Fig. 5a). Higher magnification images show that these nanoscale webs are composed of both crystalline particles and amorphous material (Fig. 5b). We find that the collection surface affects the aggregation of nanoparticles and amorphous material. For example, TEM specimen grids that are coated with an uneven, holey carbon film give rise to small clusters instead of strands of particles. These observations suggest that it may be possible to control the self-assembly of nanoparticles through the morphology of the substrate.

We studied the dependence of the size and structure of the ablated material on pressure by collecting the ablated material at various H_2 background pressures. The amount of amorphous material collected on the TEM grids increases as the pressure decreases. At 13 kPa, there is approximately three times more amorphous material than at 67 kPa. At 0.27 kPa, the collected material is nearly completely amorphous, intermixed with a few crystalline particles. The crystalline material, too, changes with pressure. Figure 6 shows the crystalline particle size distribution at two different background pressures: 13 and 67 kPa. The average size of the crystalline particles increases as the pressure decreases. At both 13 and 67 kPa, the size of the crystalline particles fits a log-normal distribution. However, the geometric mean diameter is greater for particles produced at

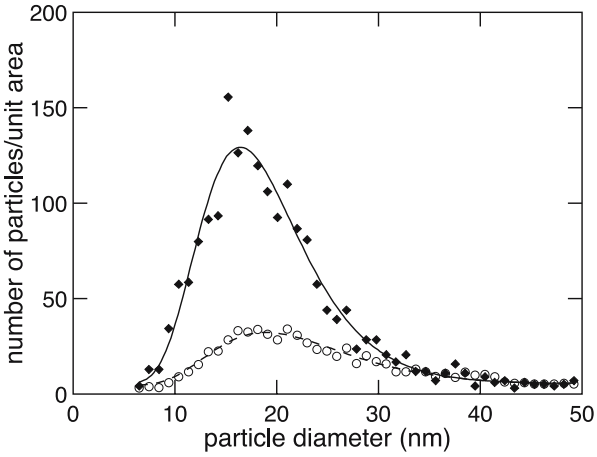

FIGURE 6 Size distribution of crystalline nanoparticles formed during femtosecond laser ablation of silicon in H_2 gas at 13 kPa (*filled diamonds*) and 67 kPa (*open circles*). The *solid* and *dashed curves* are log-normal fits with geometric means of 18.8 ± 0.2 nm and 16.2 ± 0.2 nm, and standard deviations of 0.50 ± 0.02 nm and 0.44 ± 0.02 nm, for particles formed at 13 kPa and 67 kPa, respectively

13 kPa (18.8 ± 0.2 nm) than at 67 kPa (16.2 ± 0.2 nm). At 0.27 kPa, the crystalline particles are embedded in a continuous amorphous film preventing the determination of an accurate particle size distribution.

4 Discussion

Depending on the cooling rate, liquid silicon forms either the energetically favorable crystalline phase or a metastable amorphous phase upon reaching the melting temperature [8]. At high cooling rates, such as in electrohydrodynamic atomization of silicon in vacuum [9, 10] (10^6–10^7 K/s) or after irradiation of a silicon substrate with nanosecond [11] and picosecond [12, 13] laser pulses ($\geq 10^{10}$ K/s), a metastable amorphous phase can nucleate and grow before crystallization occurs [8]. At lower cooling rates, there is sufficient time for the more stable crystalline phase to nucleate and grow.

The presence of both amorphous and crystalline silicon in the collected material indicates that the cooling rate in our experiment is near the threshold cooling rate for formation of the amorphous phase (10^6 K/s). This cooling rate is well below the estimated cooling rate for femtosecond laser ablation of silicon in vacuum (10^{12}–10^{18} K/s) [3], suggesting that the background gas lowers the cooling rate of the ejected silicon. As the background pressure is increased, the amount of crystalline material increases (Fig. 6) and the amount of amorphous material – which requires a higher cooling rate – decreases. The cooling rate within the ablation plume varies, because the mass of the silicon droplets is distributed over a range. Large liquid droplets cool by convection and radiation at a slower rate than smaller droplets. Indeed, nearly all of the crystalline particles we observe are larger in size than the amorphous particles (because of their larger size they cooled more slowly, providing enough time for crystallization).

The presence of a background gas fundamentally changes the mechanism of nanoparticle formation. In vacuum, the solid–liquid transformation is reported to be non-thermal and to take place within 50 ps [6]. This time period is too short for particles with crystalline order to form. The threshold speed for the crystalline–liquid interface above which the amorphous phase forms is reported to be 15 m/s [13]. At this speed 100-nm particles require 3 ns to form; 5-nm particles require 160 ps. We observe crystalline particles as large as 300 nm. Crystalline particles of this size can only form by a thermal process of crystal nucleation and growth.

The formation of single crystal rather than polycrystalline particles is consistent with what is known about nucleation and growth of crystalline silicon. Multiplying the volume of the mean particle, 2×10^{-24} m^3, by the largest reported [14] value for the homogeneous nucleation rate, 2×10^{10} m^{-3} s^{-1}, and inverting the result, we find that the time between two nucleation events within the volume of the mean particle is at least 10^{13} s, which is far greater than the solidification time. In other words, the observed nanoparticles solidify completely before a second nucleation event can occur and therefore they must be a single crystal.

The log-normal nature of the size distribution of the crystalline particles allows us to draw conclusions about the process of ablation in a background gas. A log-normal size distribution was first associated with the nucleation and growth of small particles during evaporation of metals in an inert gas [15]. It was recently shown that nucleation and growth of liquid droplets from the vapor phase produces a log-normal size distribution if the following four criteria are met: (1) nucleus particles (or droplets) only grow in a finite active growth region, (2) they travel through it by both drift and diffusion, (3) they are collected at a fixed point outside the active zone, and (4) their size in the active region is a power function of time [16, 17]. The ablation plume in our experiment meets all of the above criteria if we assume that it is initially composed of vapor or a mixture of liquid and vapor. Liquid droplets in the ablation plume grow while new droplets nucleate and grow through vapor condensation until the vapor phase is depleted. The finite amount of vapor establishes a finite active growth region. The kinetic energy of the ablation plume provides a condition of strong drift, in addition to diffusion, which is always present. The liquid droplets then solidify as either crystalline or amorphous depending on their cooling rate and are collected on the TEM grid. The time dependence of the size of a droplet growing by vapor condensation is linear (i.e. it is a power function in time where the exponent is unity) [16].

As the background gas pressure is decreased, the peak in the log-normal size distribution of the crystalline particles shifts to a larger particle size (Fig. 6). We can attribute this shift to an increase of the average cooling rate within the plume at lower pressures. As the cooling rate increases, more of the smaller liquid droplets become amorphous and the average size of the crystalline particles increases.

A key difference between femtosecond laser ablation in a background gas and in vacuum is the evolution of the kinetic energy of the ejected ablation plume. In a vacuum, the ejected material retains much of its kinetic energy and is eventually deposited along a line-of-sight trajectory. Many evaporation-based thin film growth techniques, such as pulsed laser deposition, rely on this process. However, in a background gas, the kinetic energy of the ejected material is reduced significantly due to interaction with the background gas. The initial kinetic energy is reduced to zero before any deposition occurs and the plume material moves about the chamber by convection. In H_2S, the ejected plume is observed to turn upward in the opposite direction of gravity. This upward turn is likely brought about by a density difference between the plume and the background gas resulting in a buoyancy effect. In H_2, the plume remains perpendicular to the target, indicating that the density of the plume is similar to H_2.

We attribute the formation of nanoscale webs to the aggregation of particles suspended in the background gas. As the plume material remains suspended in the chamber during the length of the experiment, the particles aggregate and form three-dimensional structures and clusters, which then come to rest on the TEM grids. The strands of the nanoscale webs are composed of individual aggregated nanoparticles (Fig. 5b). A recent theoretical report on coagulation of particles suspended in a gas predicts that under certain conditions particles aggregate into web-like clusters similar in shape to the clusters we observe [18]. It may be possible to form more complex three-dimensional nanostructures by controlling the gas type and pressure as well as the morphology, structure, and chemistry of the collection substrate.

In summary, the presence of a gas during femtosecond laser ablation of silicon changes the fundamental mechanism by which nanoparticles form. The background gas suppresses the non-thermal phase transformation observed in vacuum allowing some particles to crystallize through a thermal nucleation and growth process. The log-normal size distribution of crystalline particles suggests that the ablation plume contains a vapor component. The presence of the background gas also results in the suspension of plume material in the chamber for extended periods of time, resulting in the formation of long straight lines and webs of nanoparticles. The pressure and gas chemistry control the structure, composition, and size distribution of the ejected material. Our results show that it may be possible to tailor the creation of nanoparticles and control their self-assembly on a collection surface.

REFERENCES

1 A. Cavalleri, K. Sokolowski-Tinten, J. Bialkowski, M. Schreiner, D. von der Linde, J. Appl. Phys. **85**, 3301 (1999)
2 D. von der Linde, K. Sokolowski-Tinten, Appl. Surf. Sci. **154**, 1 (2000)
3 T.E. Glover, J. Opt. Soc. Am. B **20**, 125 (2003)
4 S. Amoruso, R. Bruzzese, N. Spinelli, R. Velotta, M. Vitiello, X. Wang, G. Ausanio, V. Iannotti, L. Lanotte, Appl. Phys. Lett. **84**, 4502 (2004)
5 A.V. Bulgakov, I. Ozerov, W. Marine, Appl. Phys. A **79**, 1591 (2004)
6 T.E. Glover, G.D. Ackerman, R.W. Lee, D.A. Young, Appl. Phys. B **78**, 995 (2004)
7 D.B. Williams, C.B. Carter, *Transmission Electron Microscopy* (Plenum, New York, 1996)
8 Y. Shao, F. Spaepen, D. Turnbull, Metall. Trans. A **29**, 1825 (1998)
9 Y.W. Kim, H.M. Lin, T.F. Kelly, Acta Metall. **37**, 247 (1989)
10 P.V. Evans, G. Devaud, T.F. Kelly, Y.W. Kim, Acta Metall. Mater. **38**, 719 (1990)
11 M.O. Thompson, J.W. Mayer, A.G. Cullis, H.C. Webber, N.G. Chew, J.M. Poate, D.C. Jacobson, Phys. Rev. Lett. **50**, 896 (1983)
12 P.L. Liu, R. Yen, N. Bloembergen, R.T. Hodgson, Appl. Phys. Lett. **34**, 864 (1979)
13 P.H. Bucksbaum, J. Bokor, Phys. Rev. Lett. **53**, 182 (1984)
14 G. Devaud, D. Turnbull, Appl. Phys. Lett. **46**, 844 (1985)
15 C.G. Granqvist, R.A. Buhrman, J. Appl. Phys. **47**, 2200 (1976)
16 J. Soderlund, L.B. Kiss, G.A. Niklasson, C.G. Granqvist, Phys. Rev. Lett. **80**, 2386 (1998)
17 L.B. Kiss, J. Soderlund, G.A. Niklasson, C.G. Granqvist, Nanostruct. Mater. **12**, 327 (1999)
18 M. Wilkinson, B. Mehlig, Europhys. Lett. **71**, 186 (2005)